

CHAPTER 4

MEASUREMENT OF $^{197}\text{Au}(n,\gamma)^{198}\text{Au}$ REACTION CROSS-SECTIONS USING ACTIVATION TECHNIQUE

4.1 Introduction

4.2 Experimental method

4.3 Calculations

4.3.1 Calculations of neutron flux

4.3.2 Calculations of cross-section

4.3.3 Uncertainty calculation

4.4 Calculation of $^{197}\text{Au}(n,\gamma)^{198}\text{gAu}$ reaction cross-sections

4.5 Result and discussion

4.6 Conclusions

References

Publication related to this chapter

V. Vansola, R. Ghosh, S. Badwar, B. M. Lawriniang, A. Gopalakrishna, H. Naik, Y. Naik, N. S. Tawade, S. C. Sharma, J. P. Bhatt, S. K. Gupta, S. Sarode, S. Mukherjee, N. L. Singh, P. Singh, A. Goswami

Radiochim. Acta 103, 817 (2015).

4.1 Introduction

At low energies, $^{197}\text{Au}(n,\gamma)$ reaction cross-sections are used as a neutron flux monitor, for determining the neutron activation cross-section. From the available data of Mughabghab et al. [1] in the literature, at the thermal energies, the $^{197}\text{Au}(n,\gamma)$ reaction cross-section data are known with great accuracy. However, during the operation of reactor there is a spectrum of neutron from thermal to 15 MeV energy. If one wants to use $^{197}\text{Au}(n,\gamma)$ reaction at higher energies as a flux monitor then one must have the accurate knowledge of $^{197}\text{Au}(n,\gamma)$ reaction cross-section at different neutron energies. Previously, it was a very tough task to get a neutron source with mono energetic neutrons and that to with good amount of flux, except for the D+D reaction at 2.45 MeV energy neutrons and from the T+D reaction at 14.4 MeV energy neutrons. However, with proceeding years one has gained the ability to obtain mono energetic neutrons using different reactions with good amount of flux. Among these reactions, $^7\text{Li}(p,n)$ reaction is a very good mono energetic neutron source below 6 MeV proton energy.

On the basis of the experimentally measured data available in literature, enough $^{197}\text{Au}(n,\gamma)$ reaction cross-section data in between the range of 0.025 eV to 3 MeV and at 14.7 MeV neutron energies are compiled in the EXFOR [2]. Except these data, there are no experimental data available in the literature in between 3 to 14.7 MeV neutron energies. In this context, I decided to determine the (n,γ) reaction cross-section of ^{197}Au with four different neutron energies, i.e., 1.12, 2.12, 3.12 and 4.12 MeV using the neutron activation method and off-line γ -ray spectroscopic technique. The $^{197}\text{Au}(n,\gamma)$ reaction cross-sections at the above mentioned neutron energies were computed theoretically side by side with the help of nuclear model code, TALYS [17]. The detailed comparison between theoretically and experimentally obtained data was also compared with the cross-section data available in the literature.

4.2 Experimental method

Four experiments were performed using two different accelerator facilities for the determination of $\text{Au}(n,\gamma)$ reaction cross-section at four different neutron energies. All the four experiments were performed using $^7\text{Li}(p,n)$ reaction to generate fast neutrons, with the use of 3, 4, 5 and 6 MeV proton energies. For $^7\text{Li}(p,n)^7\text{Be}$ reaction, the Q-value to the ground state is 0.431 MeV above the ground state which leads to an average Q-value of -1.868 MeV. Also for the same reaction threshold energy value to the ground state of ^7Be is 1.881 MeV. Hence, the proton energies of 3, 4, 5 and 6 MeV results into respective peak neutron energies

of 1.12, 2.12, 3.12 and 4.12 MeV peak energy of the neutrons of group one (n_0). For the first excited state of ${}^7\text{Be}$, the corresponding neutron energy of the 2nd group of neutrons (n_1) is, 0.63, 1.63, 2.63 and 3.63 MeV, respectively [18-20]. This happens due to production of n_1 group of neutrons above 2.37 MeV proton energies. Also the n_1 group of neutrons have the negligible contribution within 6 MeV proton energies, there will arise full energy peak in the neutron spectrum due to the ${}^7\text{Li}(p,n){}^7\text{Be}$ reaction and a continuum component attributable to the multi-body break up reactions, like ${}^7\text{Li}(p,n^3\text{He})\alpha$ which has Q-value of -3.231 MeV. In context to this, the main peak will cause the neutron emission of the neutron energies of 1.12 ± 0.11 , 2.12 ± 0.15 , 3.12 ± 0.21 and 4.12 ± 0.32 MeV, respectively.

The first two experiments were performed using FOTIA (Folded Tandem Ion Accelerator) at Van-De-Graff, BARC, Mumbai. For the generation of fast neutrons using the ${}^7\text{Li}(p,n){}^7\text{Be}$ reaction, a circular LiF pellet having 1 cm diameter and 3 mm thickness was used. This LiF pellet was placed on a holder inside making zero degree angle of the beam exit window. The beam collimator having a diameter of 10 mm was kept in front of the target. The current remained 100 nA constant, for neutron energies of 1.12 and 2.12 MeV. The LiF pellet, is thick enough (thickness=3 mm) for stopping the 3 and 4 MeV energy proton beams. Along with the main gold target, flux monitor In was also kept for the irradiation. Two different stacks were made for two different neutron irradiation experiments. The Au foil used during the experiment with 1.12 MeV neutrons weighed 52.7 mg and with 2.12 MeV neutrons it weighed 59.1 mg. Similarly the In foils weighed 98.8 mg and 163.7 mg for 1.12 and 2.12 MeV neutron energies experiments, respectively. All the samples are kept of the similar size $1 \times 1 \text{ cm}^2$ to avoid the size effect. Almost 100% pure gold foil was wrapped with Al foil having 0.025 mm thickness. The In foil was also wrapped separately in the other Al foil of same thickness in order to avoid the contamination of target and monitor with each other. An additional Al foil was wrapped around the Au-In stack and was kept after the LiF target with the distance of 3 mm from the LiF target. The schematic diagram of this experimental set up is given in figure 2.1 in chapter 2. These two different stacks were irradiated one by one. During the experiments, the irradiation of the samples was done for 8.6 hours and 5.6 hours for 3 and 4 MeV proton energies, respectively. All the details are given in table 4.1 and 4.2.

Table 4.1: Irradiation and sample details for FOTIA experiments

Proton energy (MeV)	Neutron Energy (MeV)	Current (nA)	Irradiation Time (hour)	Weight of Au foil (mg)	Weight of In foil (mg)	Size (cm²)
3	1.12	100	8.58	52.7	98.8	1×1
4	2.12	100	5.55	59.1	163.7	1×1

Table 4.2: Irradiation and sample details for TIFR experiments

Proton energy (MeV)	Neutron Energy (MeV)	Current (nA)	Irradiation Time (hour)	Weight of Au foil (mg)	Weight of In foil (mg)	Size (cm²)
5	3.12	50	11.8	59	58.1	1×1
6	4.12	60	13.4	59.4	64.3	1×1

Other two experiments were performed with the use of the facility of at 14UD BARC-TIFR Pelletron TIFR, Mumbai. ${}^7\text{Li}(p,n){}^7\text{Be}$ reaction is used to generate the fast neutrons of energies of 3.12 and 4.12 MeV with the help of proton beams of 5 and 6 MeV energies, respectively [22]. The currents during these two irradiations were 50 nA and 60 nA for 5 and 6 MeV proton energies, respectively. These experiments were carried out at 6m height up the analyzing magnet of the BARC-TIFR Pelletron facility so that the current can be exploited to its maximum potential. Generating voltage mode (GVM) regulates the terminal voltage with the use of a terminal potential stabilizer. Before the target, 6 mm diameter beam collimator was used. Natural lithium foil with thickness 3.7 mg/cm^3 was kept in between the two tantalum foils possessing different thicknesses. The tantalum foil, which faces proton beam is the thinnest with the thickness of 3.9 mg/cm^3 and the tantalum foil which stops the beam is the thickest, having thickness of 0.025 mm. Energy degradation of the proton beam due to thinnest tantalum foil is around 50-85 keV [23]. For the irradiation with 5 MeV proton beam gold foil having the weight 59 mg and Indium foil with the weight 58.1 mg were wrapped with the 0.025 mm thick aluminium foil separately. Similarly, for the irradiation with 6 MeV proton beam gold foil having the weight 59.4 mg and Indium foil with the weight 64.3 mg are wrapped with the 0.025 mm aluminium foil separately. As mentioned above, all the samples are kept of the similar size $1 \times 1 \text{ cm}^2$ to avoid the size effect. These Au-In stacks were mounted at 2.1 cm distance behind the Ta-Li-Ta stack at zero degree angled with respect to the proton beam direction [22]. The schematic diagram of this experimental set up is given in figure 2.2 in chapter 2. The samples are then irradiated with the neutron beam generated by 5 and 6 MeV proton energies for 11.8 h and 13.4 h respectively.

After the irradiation in all the experiments, Au samples were cooled for 2.3 hour to 19 hour and In samples were cooled for 0.7 hour to 19 hour. The neutron irradiated samples based on the proton energies of 5 and 6 MeV were cooled for 0.7 and 1.25 hours, respectively. After cooling, γ -ray counting of all the samples was done with the help of pre-calibrated 80 cm^3 HPGe detector counting system directly connected with a PC based 4096 multi-channel analyser. ${}^{152}\text{Eu}$ standard source was used for the energy and efficiency calibration of the HPGe detector. Before the counting, the resolution of the detector was calculated which turned out to be 2.0 keV at 1332 keV γ -energy of ${}^{60}\text{Co}$. Typical γ -ray spectra of irradiated Au and In samples are given in figures 4.1 and 4.2, respectively.

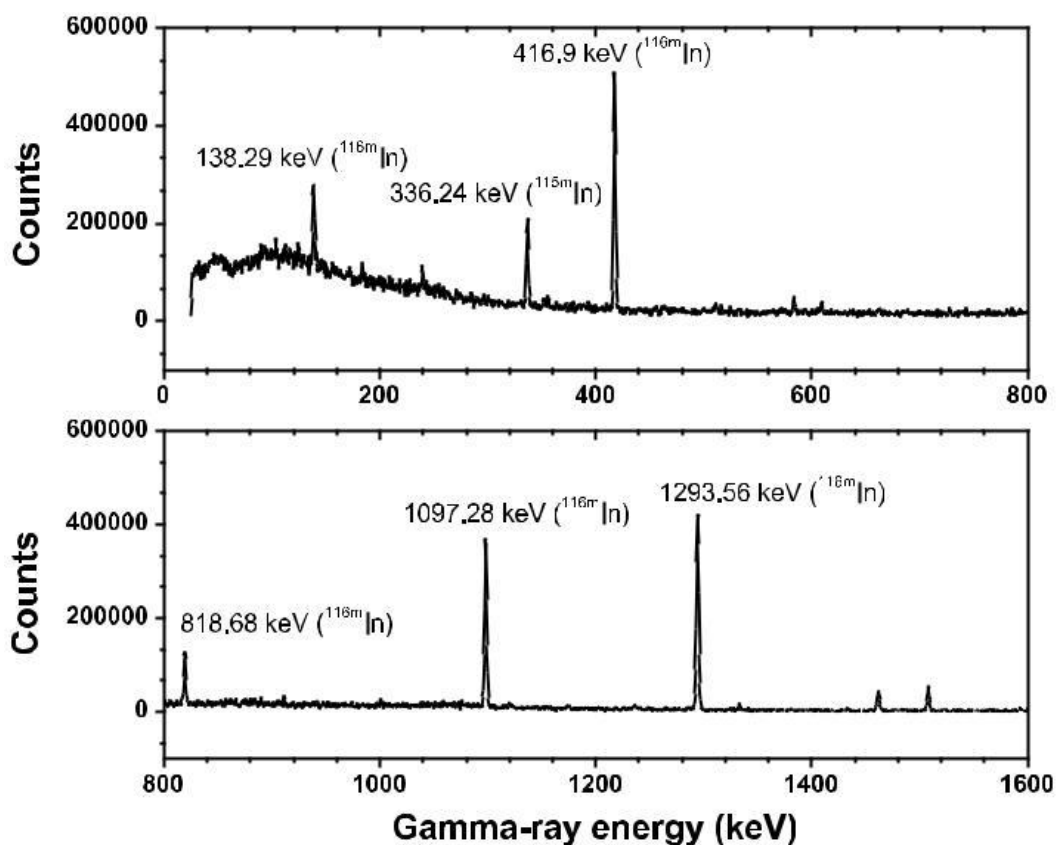


Figure 4.1: Gamma-ray spectrum of activated ^{nat}In foil with the neutron energy of 1.12 MeV; irradiation time= 8.58 h, cooling time=42 min and counting time=10 min

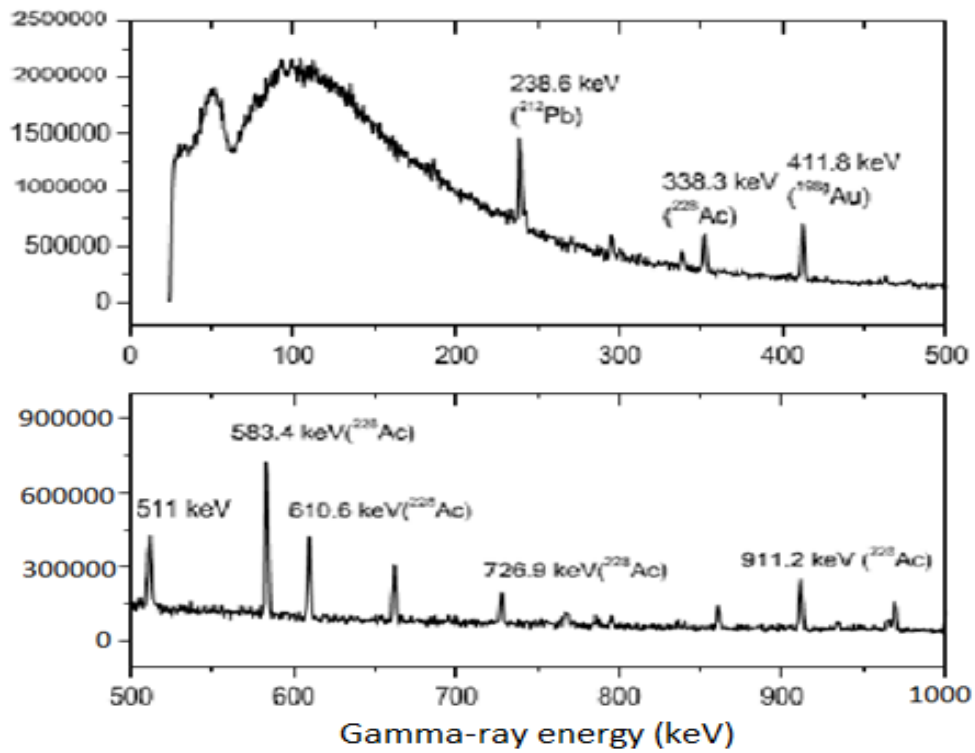


Figure 4.2: Gamma-ray spectrum of activated ^{197}Au foil with the neutron energy of 2.12 MeV; irradiation time= 5.55 h, cooling time=44.47 h and counting time=3.216 h

4.3 Calculations

4.3.1 Calculation of neutron flux

From the photo-peak activity (A) of 138.33, 416.86, 818.72, 1097.33 and 1293.56 keV γ – lines of $^{116\text{m}}\text{In}$, the neutron flux (ϕ) was calculated by using Equation 2.3 from chapter 2 [21].

Where, σ_R = the cross-section of the $^{115}\text{In}(n, \gamma)^{116\text{m}}\text{In}$ reaction

$$\lambda = \text{the decay constant } \left(\lambda = \frac{\ln 2}{T_{1/2}} \right) \text{ of the reaction product } ^{116\text{m}}\text{In} \text{ with half-life} = 54.29$$

min, I_γ is the branching intensity of the 138.33, 416.86, 818.72, 1097.33 and 1293.56 keV γ – line of $^{116\text{m}}\text{In}$ [24].

In the literature $^{115}\text{In}(n, \gamma)^{116\text{m}}\text{In}$ reaction cross-section is available for a wide range of neutron energies [25–35]. However, within the neutron energy range of 1.96 to 7.66 MeV, the $^{115}\text{In}(n, \gamma)^{116\text{m}}\text{In}$ reaction cross-sections are available in the refs. [30, 32, 33, 35]. Among all these literature data, the cross-section data by Husain et al. [32] fall within 2.44 to 4.5 MeV neutron energy range but, are higher, than the other data available in the literature by different authors [30, 33, 35]. Thus for the neutron flux calculation, $^{115}\text{In}(n, \gamma)^{116\text{m}}\text{In}$ reaction cross-sections from the refs. [30, 33, 35] were used in the present work. The computed $^{115}\text{In}(n, \gamma)^{116\text{m}}\text{In}$ reaction cross-sections as a function of neutron energy using different nuclear model codes are available in ref. [36]. Thus the evaluated $^{115}\text{In}(n, \gamma)^{116\text{m}}\text{In}$ reaction cross-sections were also used for determining the neutron flux in the present work.

4.3.2 Calculation of cross-section

To calculate the $^{197}\text{Au}(n, \gamma)^{198\text{g}}\text{Au}$ reaction cross-section by equation 2.20 in chapter 2, the neutron flux obtained from above described method was used. The photo-peak activity of the 411.8 keV γ – ray of $^{198\text{g}}\text{Au}$ were used. Reference [24] provides the nuclear spectroscopic data used in the above calculations and are presented in Table 4.3.

Table 4.3: Nuclear spectroscopic data of the radio-nuclides from the $^{197}\text{Au}(n,\gamma)^{198g}\text{Au}$ and $^{115}\text{In}(n,\gamma)^{116m}\text{In}$ reactions used in the calculation from Ref. [24]

Nuclide	Spin-Parity	Half life	Decay Mode	γ -ray Energy in keV	γ -ray Abundance in %
$^{116m}_{49}\text{In}$	5+	54.29±17 min	β^- :100%	138.33	3.7
				416.86	27.2
				818.72	12.13
				1097.33	58.5
				1293.56	84.8
$^{198g}_{79}\text{Au}$	2-	2.6948±4 days	β^- :100%	411.8	95.62

Since the neutron spectrum has some tail, it affects $^{197}\text{Au}(n,\gamma)^{198\text{g}}\text{Au}$ reaction cross-section. At the same time, it also affects the $^{115}\text{In}(n,\gamma)^{116\text{m}}\text{In}$ monitor reaction cross-section. This is because both the $^{115}\text{In}(n,\gamma)^{116\text{m}}\text{In}$ and $^{197}\text{Au}(n,\gamma)^{198\text{g}}\text{Au}$ reaction cross-sections decrease with neutron energy. The contribution of small tail part in the reaction cross-section is discussed in the next section given below.

4.3.3 Uncertainty calculation

Cross-sections for the $^{197}\text{Au}(n,\gamma)^{198\text{g}}\text{Au}$ reaction were determined at 1.12, 2.12, 3.12 and 4.12 MeV neutron energies and the values are given in Table 4.4. Because of systematic as well as statistical errors the measured cross-section values contain some uncertainties. The overall uncertainty is the quadratic sum of both statistical and systematic errors. The random error in the observed activity arises mainly because of the counting statistics, which is estimated to be 3.1 % – 5.5 % for $^{198\text{g}}\text{Au}$. This can be computed by the accumulation of the data for an optimum time period, which is dependent on the nuclide's half-life. Uncertainties in the irradiation time ($\sim 0.1\%$), half-life of the reaction product, γ -ray abundance ($\sim 2\%$) and detection efficiency ($\sim 3\%$), adds up to be the systematic errors. Detection efficiency arises from the fitting error. Hence, total systematic error is approximately $\sim 3.6\%$. From both statistical as well as systematic errors the combined uncertainties lie within $4.8\% - 6.6\%$ for the $^{197}\text{Au}(n,\gamma)^{198\text{g}}\text{Au}$ reaction cross-section. The energy degradation of the proton beam energy might get caused within the lithium metal foil. The $^{115}\text{In}(n,\gamma)^{116\text{m}}\text{In}$ monitor reaction cross-section can cause uncertainty in the flux and that will reflect in the $^{197}\text{Au}(n,\gamma)^{198\text{g}}\text{Au}$ reaction cross-section. However, neutron energy uncertainty rising because of the different extent of population of n_0 and n_1 groups of neutrons is more prominent than above mentioned uncertainty.

4.4 Calculation of $^{197}\text{Au}(n,\gamma)^{198\text{g}}\text{Au}$ reaction cross-sections

The protons falling on the Lithium will cause a neutron spectrum with different energies. These neutron spectra of all the four experiments from $^7\text{Li}(p,n)$ reaction at the proton energies of 3, 4, 5 and 6 were calculated [19–22] and the results are plotted in figure 4.3. As mentioned above, the neutron spectrum consists of the full energy peak. $^7\text{Li}(p,n)^7\text{Be}$ reaction and a continuum component will cause multi-body break up process, i.e., $^7\text{Li}(p,n^3\text{He})\alpha$, which has Q-value of -3.231 MeV.

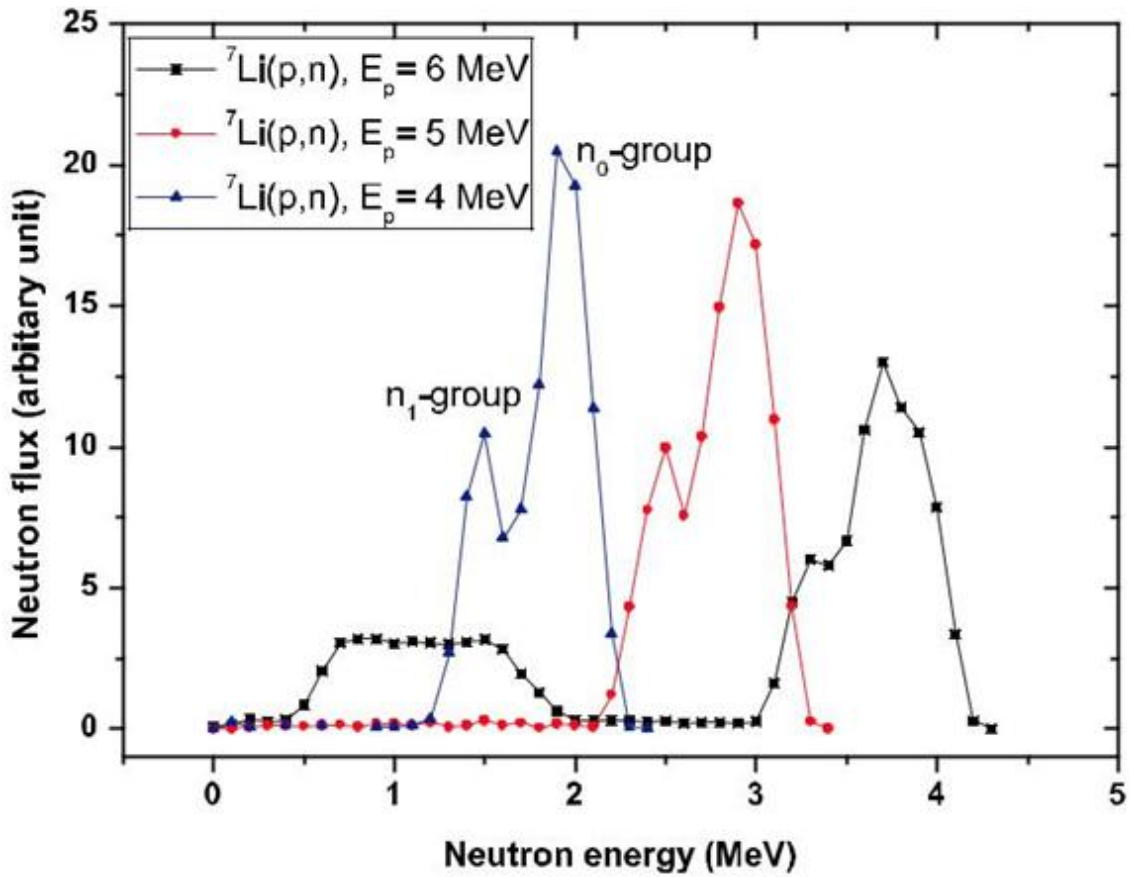


Figure 4.3: Neutron spectra from the ${}^7\text{Li}(p,n)$ reaction with proton energies of 4, 5 and 6 MeV [37]

This case applies to the protons of 6 MeV energy and not for the protons of 3 to 5 MeV energy, because at low energies one will have almost mono energetic neutrons because of the domination of ${}^7\text{Li}(p,n){}^7\text{Be}$ reaction. However, different extent of population of n_0 and n_1 groups of neutrons, which causes the broadening of the neutron spectrum can be seen clearly in the figure 4.3.

When proton beam of 6 MeV energy cause the neutron spectrum, it will have tailing at low energy. This tail affects the cross- section of the ${}^{115}\text{In}(n, \gamma){}^{116m}\text{In}$ reaction monitor and so the ${}^{197}\text{Au}(n,\gamma){}^{198g}\text{Au}$ reaction. To know the exact value of tailing, the ${}^{197}\text{Au}(n,\gamma){}^{198g}\text{Au}$ and ${}^{115}\text{In}(n,\gamma){}^{116m}\text{In}$ reaction cross-sections were theoretically calculated by using TALYS 1.6 [17] so the tailing part can be subtracted. Hence, TALYS calculation was done by using the default parameters for the neutron energies of 10 keV to 20 MeV with ${}^{115}\text{In}$ and ${}^{197}\text{Au}$ as targets. All possible outgoing channels for this particular entrance channel were taken into account including (n,γ) and inelastic reactions. From all the reactions, the (n,γ) reaction cross-sections within the neutron energy of 10 keV to 20 MeV were selected on the basis of half-life of the product nuclide, gamma-ray intensities and several other parameters. TALYS code deals with the theoretical reaction cross-sections for the mono-energetic neutrons. Thus we had to take the flux-weighted average of the ${}^{197}\text{Au}(n,\gamma){}^{198g}\text{Au}$ and ${}^{115}\text{In}(n,\gamma){}^{116m}\text{In}$ reaction cross-sections ($\langle\sigma_R\rangle$) and were calculated using equation (4.1) as given in ref. [22]. The ${}^{197}\text{Au}(n,\gamma){}^{198g}\text{Au}$ and ${}^{115}\text{In}(n,\gamma){}^{116m}\text{In}$ reaction cross-sections at different neutron energy.

$$\langle\sigma_R\rangle = \sum \sigma_R \phi / \sum \phi \quad (4.1)$$

With the neutron spectrum given in figure 4.4 and theoretical values from TALYS, the flux-weighted average the ${}^{197}\text{Au}(n,\gamma){}^{198g}\text{Au}$ and ${}^{115}\text{In}(n,\gamma){}^{116m}\text{In}$ reaction cross- sections for the neutron energy of 4.12 MeV were obtained as 53.141 mb and 45.692 mb, respectively. By taking the theoretical flux-weighted average ${}^{115}\text{In}(n,\gamma){}^{116m}\text{In}$ reaction cross-section of 53.141 mb and the photo-peak activity of 411.8 keV γ -ray of ${}^{198g}\text{Au}$, the ${}^{197}\text{Au}(n,\gamma){}^{198g}\text{Au}$ reaction cross-section turned out to be 47.506 mb. This value of cross-section is close to the theoretical flux-weighted average the ${}^{197}\text{Au}(n,\gamma){}^{198g}\text{Au}$ reaction cross-section of 45.692 mb. So at 4.12 MeV neutron energy, the experimental ${}^{115}\text{In}(n,\gamma){}^{116m}\text{In}$ reaction cross-section of 16.7 mb [33] and the photo-peak activity of 411.8 keV γ -ray of ${}^{198g}\text{Au}$, the ${}^{197}\text{Au}(n,\gamma){}^{198g}\text{Au}$ reaction cross-section obtained as 14.926 mb seems quite reasonable. This is because of the characteristics of (n,γ) reaction cross-sections. Thus, both the ${}^{197}\text{Au}(n,\gamma){}^{198g}\text{Au}$ and

$^{115}\text{In}(n,\gamma)^{116\text{m}}\text{In}$ reaction cross-sections decrease collaterally with the increase of neutron energy. So with the use of the $^{197}\text{Au}(n,\gamma)^{198\text{g}}\text{Au}$ reaction cross-section as the neutron flux monitor, the contribution to the $^{197}\text{Au}(n,\gamma)^{198\text{g}}\text{Au}$ reaction cross-section due to the tailing part in the neutron spectrum was avoided. On the basis of this argument, one can say that the $^{197}\text{Au}(n,\gamma)^{198\text{g}}\text{Au}$ reaction cross-sections shown in table 4.4 with the use of the experimental $^{115}\text{In}(n,\gamma)^{116\text{m}}\text{In}$ reaction cross-sections at the neutron energies of 1.12–4.12 MeV are reasonable. Proton energies of 3, 4 and 5 MeV do not cause any tailing in the neutron spectra. Hence, there is clearly no need of any kind of tailing corrections for the $^{197}\text{Au}(n,\gamma)^{198\text{g}}\text{Au}$ reaction cross-section at the neutron energies of 1.12, 2.12 and 3.12 MeV.

4.5 Results and discussion

The cross-sections of the $^{197}\text{Au}(n,\gamma)^{198\text{g}}\text{Au}$ reaction at four different neutron energies of 1.12, 2.12, 3.12 and 4.12 MeV were measured in the present work for the first time. There isn't any available nuclear reaction cross-section data in the literature [5–16] within the neutron energy range of 3–4.5 MeV. However, there are some nuclear cross-section data available at the neutron energy of 0.025 eV [1–3], within 0.2–3 MeV [7–13, 16] and at 14.7 MeV [14, 15] in literature. The experimental data calculated experimentally in the present work at 1.12 and 2.12 MeV neutron energies lie in between the values within the neutron energies of 1 to 1.2 MeV and 2 to 2.2 MeV, respectively. However, the experimental values of cross-sections at all four neutron energies are higher than the evaluated $^{115}\text{In}(n,\gamma)^{116\text{m}}\text{In}$ reaction cross-sections [36]. In accordance to this, the theoretical reaction cross-sections of the $^{197}\text{Au}(n,\gamma)^{198\text{g}}\text{Au}$ from the computation of TALYS 1.6 at 1.12, 2.12, 3.12 and 4.12 MeV neutron energies are also shown in Table 4.4. From Table 4.4, It is quite clear that the experimentally determined cross-sections of the $^{197}\text{Au}(n,\gamma)^{198\text{g}}\text{Au}$ reaction in the present work at the neutron energies of 1.12 and 4.12 are in general agreement with the theoretically computed values of TALYS 1.6 [17]. However, the cross-sections of the $^{197}\text{Au}(n,\gamma)^{198\text{g}}\text{Au}$ reaction at the neutron energies of 2.12 and 3.12 MeV are lower than the computed values of theoretical code TALYS 1.6. From the Table 4.4, it is also clear that the theoretical values of the $^{197}\text{Au}(n,\gamma)^{198\text{g}}\text{Au}$ reaction cross-sections computed using TALYS 1.6 code are higher than the $^{197}\text{Au}(n,\gamma)^{198\text{g}}\text{Au}$ reaction sections based on the evaluated $^{115}\text{In}(n,\gamma)^{116\text{m}}\text{In}$ reaction cross-sections. Figure 4.4 shows the comparison of the present experimental data at four neutron energies, theoretically evaluated data using TALYS 1.6 within the 10 keV to 20 MeV as well as the literature data [3–16] at other neutron energies. From figure 4.4, it is clear that, within

the neutron energies of 2.12 –4.12 MeV, the experimentally measured data in the present work and the data available in the literature [7–13] are slightly lower than the computed values based on nuclear model code TALYS 1.6 but they follow quite similar trend. The theoretical values are systematically higher than the experimental values of the $^{197}\text{Au}(n,\gamma)^{198\text{g}}\text{Au}$ reaction cross-section data at other neutron energies.

The $^{197}\text{Au}(n,\gamma)^{198\text{g}}\text{Au}$ reaction cross-section data at different neutron energies with high accuracy is important because of its application as a neutron flux monitor during the determination of other reaction cross-section measurements. In IAEA, the $^{197}\text{Au}(n,\gamma)^{198\text{g}}\text{Au}$ reaction cross-section as a function of neutron energy is standard reaction monitor among all the nine standard reaction monitors. All the standard reaction monitors in IAEA are based on the IAEA reaction cross-section standards, the uncertainties for the neutron capture cross-section of Au should be within 1.4 % – 2.2 %. Since the measurements of $^{197}\text{Au}(n,\gamma)^{198\text{g}}\text{Au}$ reaction cross-sections done in the present work have the uncertainty on the higher side. Besides this, the experimentally measured $^{197}\text{Au}(n,\gamma)^{198\text{g}}\text{Au}$ reaction cross-section data is useful in testing the theoretical TALYS model.

4.6 Conclusion

In the present work, we have successfully determined the $^{197}\text{Au}(n,\gamma)^{198\text{g}}\text{Au}$ reaction cross-section at 1.12, 2.12, 3.12 and 4.12 MeV neutron energies with the use of neutron activation method and the off-line γ -ray spectrometric technique. The values at the neutron energies of 3.12 and 4.12 MeV are experimentally measured for the first time. Present data at the neutron energies of 1.12 and 2.12 MeV are in very good agreement with the data already available in the literature. The $^{197}\text{Au}(n,\gamma)^{198\text{g}}\text{Au}$ reaction cross-section were also computed theoretically using the computation code TALYS 1.6 as a function of neutron energy. All the present measured values as well as computed data were plotted along with the available experimental data in the literature and shown in figure 4.4.

Table 4.4: $^{197}\text{Au}(n,\gamma)^{198\text{g}}\text{Au}$ and $^{115}\text{In}(n,\gamma)^{116\text{m}}\text{In}$ reaction cross-sections at different neutron energies and neutron flux

		$^{115}_{49}\text{In} (n, \gamma) ^{116\text{m}}_{49}\text{In}$		$^{197}_{79}\text{Au} (n, \gamma) ^{198\text{g}}_{79}\text{Au}$	
Proton Energy (MeV)	Neutron Energy (MeV)	Cross-section (mb)	Flux (n/cm ² sec)	Cross-section	
				Experimental (mb) [Experimental ref.]	TALYS-1.6 (mb)
3	1.12±0.12	174.40±6.70	$(9.42 \pm 0.12) \times 10^6$	60.44±3.40	82.87
		[35]		85.64±4.82	
		247.09		82.50±3.50 [12]	
4	2.12±0.15	104.10±4.50	$(2.26 \pm 0.16) \times 10^7$	40.59±3.06	79.87
		[35]		50.31±3.80	
		129.00		56.30±2.40 [12]	
5	3.12±0.21	37.50±1.50 [35]	$(2.24 \pm 0.27) \times 10^7$	19.77±2.67	41.25
		44.60		23.51±3.18	
				25.00±1.10 [12]	
6	4.12±0.32	15.60±0.70 [35]	$(3.06 \pm 0.32) \times 10^7$	13.94±1.61	19.18
		16.65		14.93±1.73	
				$(2.86 \pm 0.30) \times 10^7$	

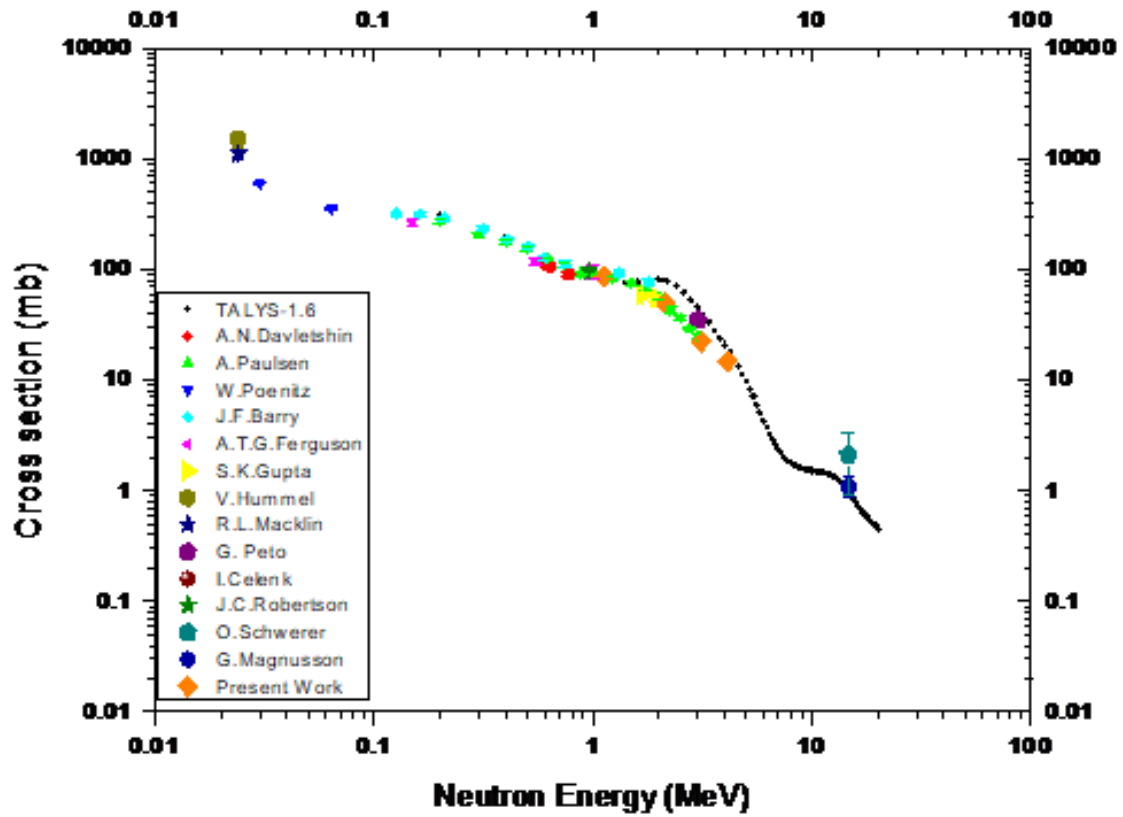


Figure 4.4: Plot of the present experimental and theoretical $^{197}\text{Au}(n,\gamma)^{198g}\text{Au}$ reaction cross-section values as well as the experimental data available in the literature, as a function of the neutron energy. Measured values in the present work and from references [3–16] are in different symbols and colour, whereas the theoretical values from TALYS are in solid square.

References:

1. A. D. Carlson, V. G. Pronyaev, D. L. Smith, N. M. Larson, Zhenpeng Chen, G. M. Hale, F. J. Hamsch, E. V. Gai, Soo-Youl Oh, S. A. Badikov, T. Kawano, H. M. Hofmann, H. Vonach, S. Tagesen, International Evaluation of Neutron Cross-section Standards. Nucl. Data Sheets **110**, 3215 (2009).
2. IAEA-EXFOR Database, available at <http://www-nds.iaea.org/exfor>.
3. D. Antonini, P. Moiola, E. Pedretti, R. Scafe, A. Isentin, Nucl. Instrum. Meth. In Phys. Res. **115**, 567 (1978).
4. I. Celenk, H. Demirel, A. Ozmen, J. Radio anal. Nucl. Chem. **148**, 393 (1991).
5. V. Hummel, B. Hamermesh, Phys. Rev. **82**, 67 (1951).
6. R. L. Macklin, N. H. Lazar, W. S. Lyon, Phys. Rev. **107**, 504 (1957).
7. A. T. G. Ferguson, E. B. Paul, J. Nucl. Energy A (Reactor Science) **10**, 19 (1959).
8. J. F. Barry, J. Nucl. Energy A & B (Reactor Sci. and Tech.) **18**, 491 (1964).
9. W. Poenitz, J. Nucl. Energy A & B (Reactor Sci. and Techn.) **20**, 825 (1966).
10. P. Peto, Z. Milligy, I. Hunyadi, J. Nucl. Energy **21**, 797 (1967).
11. J. C. Robertson, T. B. Ryves, E. J. Axton, L. Goodier, A. Williams, J. Nucl. Energy **23**, 205 (1969).
12. A. Paulsen, R. Widera, H. Liskien, Atomk ernenergie **26**, 80 (1975).
13. S. K. Gupta, J. Frehaut, R. Bois, Nucl. Instrum. Meth. in Phys. Res. **148(1)**, 77 (1978).
14. O. Schwerer, M. Winkler-Rohatsch, H. Warhanek, G. Wikler, Nucl. Phys. A **264**, 105 (1976).
15. G. Magnusson, P. Andersso, I. Berqvist, Phys. Scripta **21**, 21 (1980).
16. A. N. Davletshin, V. N. Korytchenko, A. O. Tipunkov, S. V. Tikhonov, V. A. Tolstikov, Atomic Energy **65(5)**, 913 (1988).
17. A. J. Koning, TALYS user manual, A nuclear reaction program, User manual NRG-1755 ZG PETTEN, The Netherlands (2011).
18. Rajnikant Makwana, S. Mukherjee, P. Mishra, H. Naik, N. L. Singh, M. Mehta, K. Katovsky, S. V. Suryanarayana, V. Vansola, Y. Santhi Sheela, M. Karkera, R. Acharya and S. Khirwadkar, Physical Review C **96**, 024608 (2017).
19. H. Liskien, A. Paulsen, At. Data Nucl. Data Tables **15**, 57 (1975).
20. C. H. Poppe, J. D. Anderson, J. C. Davis, S. M. Grimes, C. Wong, Phys. Rev. C **14**, 438 (1976).
21. J. W. Meadows, D. L. Smith, Neutrons from proton bombardment of natural Lithium, Argonne National Laboratory Report ANL-7983, (1972).
22. H. Naik, P. M. Prajapati, S. V. Suryanarayana, K. C. Jagadeesan, S. V. Thakare, D. Raj, V.

- K. Mulik, B. S. Sivashankar, B. K. Nayak, S. C. Sharma, S. Mukherjee, S. Singh, A. Goswami, S. Ganesan, V. K. Manchanda, *Eur. Phys. J. A.* **47(51)**, 1 (2011).
23. J. F. Ziegler, SRIM-2003. *Nucl. Instrum. Methods Phys. Res., Sect. B, Beam Interact.* **219–220**, 1027–1036 (2004), available at <http://www.srim.org/>.
24. NuDat 2.6, National Nuclear Data Center, Brookhaven National Laboratory, updated 2011, available at <http://www.nndc.bnl.gov/>.
25. H. A. Grench, H. O. Menlove, *Phys. Rev.* **165**, 1298 (1968).
26. K. Ponnert, G. Magnusson, I. Bergqvist, *Phys. Scripta* **10**, 35 (1974).
27. G. Peto, J. Csikai, V. Long, S. Mukherjee, J. Banhalmi, Z. Miligy, *Acta Phys. Slovaca*, **25**, 185 (1975).
28. W. Mannhart, *ger. Zeitschrift fuer Physik A, Hadrons and Nuclei* **272**, 273 (1975).
29. G. Magnusson, I. Bergqvist, *Nucl. Tech.* **34**, 114 (1977).
30. P. Andersson, R. Zorro, I. Bergqvist, *Conf. on Nucl. Data for Sci. And Technol.*, Bock- hoff, K. H. (editor), Antwerp, Belgium, page 866, Published by D. Reidel Publishing Company, P. O. Box 17, 3300 AA Dordrecht, Holland (1982).
31. V. L. Demekhin, B. E. Leshchenko, V. K. Majdanjuk, G. Peto, *Sixth All-Union Conf. on Neutron Physics* **3**, Kiev, 2–6 Oct., 195 (1983).
32. H. A. Husain, *Int. J. Applied Radiation and Isotopes* **34**, 731 (1983).
33. P. Andersson, R. Zorro, I. Berqvist, M. Herman, A. Marcinkowski, *Nucl. Phys. A* **443**, 404 (1985).
34. D. J. Grady, G. F. Knoll, J. C. Robertson, *Nucl. Sci. Eng.* **94**, 227 (1986).
35. R. P. Gautam, R. K. Singh, I. A. Rizvi, M. Afzal Ansari, A. K. Chaubey, S. Kailas, *Indian J. Pure and Applied Phys.* **28**, 235 (1990).
36. K. I. Zolotarev, P. K. Zolotarev, *Progress Report on Research Contract No 16242, INDC(NDS)-0657*, available at <https://www-nds.iaea.org/publications/indc/indc-nds-0657.pdf> (2013).
37. Siddharth Parashari, Surjit Mukherjee, Rajnikant Makwana, N. L. Singh, Ratan K. Singh, H. Naik, S. V. Suryanarayana, B. K. Nayak, S. C. Sharma, Mayur Mehta, Sai Akhil Ayyala, Jan Varmuza, Karel Katovsky, 19th International Scientific Conference on Electric Power Engineering (EPE), 10.1109/EPE.2018.08395960 (2018).